

## Study of the fracture behavior of different structures by the extended finite element method (X-FEM)

Zagane Mohammed El Sallah<sup>\*1,2</sup>, Moulgada Abdelmadjid<sup>1,2</sup>, Sahli Abderahmane<sup>2</sup>,  
Baltach Abdelghani<sup>1</sup> and Benouis Ali<sup>2,3</sup>

<sup>1</sup>Department of Mechanical Engineering, University of Tiaret, City Zaâroua BP 78, Tiaret 14000, Algeria

<sup>2</sup>Laboratory LMPM, University of Sidi Bel Abbes, BP 89, City Ben Mhidi, Sidi Bel Abbes 22000, Algeria

<sup>3</sup>University of Moulay, Tahar Saida, City Ennasr, BP 138 20000 Saïda, Algeria

(Received March 24, 2022, Revised March 11, 2023, Accepted May 10, 2023)

**Abstract.** The fracture mechanics make it possible to characterize the behavior with cracking of structures using parameters quantifiable in the sense of the engineer, in particular the stress field, the size of the crack, and the resistance to cracking of the material. Any structure contains defects, whether they were introduced during the production of the part (machining or molding defects for example). The aim of this work is to determine numerically by the finite element method the stress concentration factor  $K_t$  of a plate subjected to a tensile loading containing a lateral form defect with different sizes: a semicircle of different radii, a notch with different opening angles and a crack of different lengths. The crack propagation is then determined using the extended finite element technique (X-FEM). The modeling was carried out using the ABAQUS calculation code.

**Keywords:** crack; finite element method; stress concentration factor  $K_t$ ; X-FEM

### 1. Introduction

Modeling and prediction of the behavior of aeronautical and aerospace structures is a hot topic, especially for damaged structures. This damage is due to faults in the structure. Essentially, the determination of approximate solutions by the finite element method (FEM) is an expensive task, especially for complex geometries. Indeed, to obtain optimum precision, the geometry is modeled by an adequate mesh. In addition, the modeling of holes and inclusions presents another form of problem where simulation is not only costly in terms of computation but also results in loss of precision when data is mapped from an old to a new mesh during computation. Therefore, the extended finite element method (XFEM) is a numerical technique, which allows the integration of local enrichment of approximation spaces. Primarily, this latter is achieved through the notion of partition of unity. First, the researcher Pathak *et al.* (2013) used the finite element method for the simulation of components in the presence of cracks. In addition, the advantage of using X-FEM makes it possible to simulate both stationary and propagation cracks. D'Angela *et al.* (2021)

---

\*Corresponding author, Ph.D., E-mail: mohammedelsallah.zagane@univ-tiaret.dz

investigated and correlated the discrepancy between the numerical and analytical estimations of the fatigue life of the components to the features of the testing/modeling. Benzaama *et al.* (2018) presented two parameters, the first, the form of the notch in order to see its effect on the stress and the failure load, and the second, the influence of the locale orientation of fiber around the plate's notch; and concluded that it is important to optimize the effect of fiber orientation around the notch. Gasmi *et al.* (2019) resulted that cracks can only be initiated from the sharp edges of an ellipsoidal cavity in which the ratio of the minor axis over the major axis is equal to 0.1. A maximum crack length of 19  $\mu\text{m}$  was found for a cavity situated in the proximal zone position under static loading. Karamloo *et al.* (2019) presented three crack arrest methods (drilling stop-hole, steel welded patch, and carbon fiber reinforced (CFRP) patch), compared to the extended finite element method (X-FEM). The results showed that using symmetrically welded metal patches resulted in a 21% increase in fatigue life compared to symmetrical stop holes. It does not require determining the initial crack or defining the crack path Kozłowski *et al.* (2016). Several types of research were carried out with the aim of comparing and validating the numerical results obtained by the extended finite element method (X-FEM) and the results obtained experimentally Taghezout *et al.* (2020). Srivastava *et al.* (2016) typical numerical results are given to investigate the effect of specimen thickness, characteristic length, crack inclination, and mode I crack displacement distance on the fracture parameters of multiple crack configurations. Nguyen *et al.* (2018) proposed a model of multi-crack growth prediction and introduced a new technique for adjusting the maximum crack increment, as opposed to the use of a fixed maximum crack incremental as adopted by many models available in the literature, at each iterative step of crack growth simulations. Khatri *et al.* (2018) used the X-FEM method with SOPT, the stochastic fracture behavior of the analyzed model with biaxiality ratio ( $\beta=0, 1$  and  $-1$ ) is predicted by evaluating the mixed mode stress intensity factor MMSIFs and their corresponding coefficient of variations COVs for quantifying the true response towards integrity and safe working of the plate and its reliability. Khatri *et al.* (2018) examined the crack propagation behavior of thin rectangular mortar plate specimens, either with two different widths, that include artificially-prefabricated cracks on a single specimen side to facilitate unilateral crack propagation or on both sides to facilitate bilateral crack propagation under direct tensile stress, and they analyzed crack propagation interaction processes and presented associated stress-strain curves. Huang *et al.* (2017) analyzed the SIFs of stiffened plates theoretically in linear elastic fracture mechanics, then, they employed 3D FEM to conduct crack propagation analyses in three kinds of stiffened plates, next, they investigated at different situations the crack arrest effects of stiffeners and the influences of out of plane bending. The X-FEM was first applied by Sedmak (2016) is to the three-point bending specimens to verify numerical results with the experimental ones. Pereira *et al.* (2019) presented a numerical simulation with two-dimensional models created in Abaqus software were performed, and the results obtained were compared with the analytical and experimental results. Campilho *et al.* (2019) used the extended finite element method (X-FEM) to predict the crack trajectory under different loading conditions. In addition, the X-FEM predictive capabilities were tested with different damage initiation and propagation criteria. It was found that provided, that the modeling conditions are properly set, accurate numerical results can be found. Đorđević *et al.* (2021) investigated the extensive analysis and developed a simple, approximated numerical model, with the goal of determining the location of stress concentration in the support lever, so that it could be compared to the real failure location. Nassiraei *et al.* (2020) resulted that that the SCF of an FRP reinforced T/Y-joint can be down to 34% of the SCF of the corresponding unreinforced joint. Also, two parametric formulas were proposed for determining the SCFs in T/Y-joints

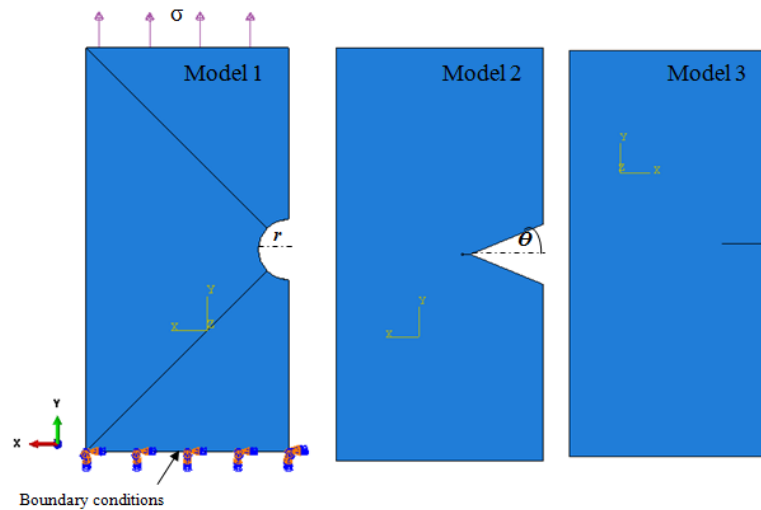


Fig. 1 Model plate geometry and boundary conditions of the different models studied

reinforced with FRP, and used to propose a design equation for determining the SCFs in T/Y-joints reinforced with different FRP materials under OPB load. Hossein *et al.* (2021) investigates the stress concentration factors (SCFs) in tubular X-connections retrofitted with fiber-reinforced polymer (FRP) under compressive load and under in-plane bending. They found that the rise of the FRP sheet number causes a considerable drop in the SCFs, also, they checked the proposed equations according to the UK DoE acceptance standard. Nassiraei *et al.* (2021) resulted that for certain geometrical parameters set, the SCF in an X-connection retrofitted with carbon fiber reinforced polymer (CFRP) can be down to 23% of the SCF in the associated un-retrofitted connection. Hossein *et al.* (2021) investigated on the (SCFs) in tubular T-joints reinforced with external ring under in-plane bending (IPB) moment. After validation of the FE model with experimental results, a set of 156 3D FE models was generated and analyzed to parametrically investigate the effect of the ring and joint geometry on the SCFs and SCF ratios.

This paper presents numerical studies on the failure behavior of three models. The first model is a plate with a semicircular lateral notch, the second is a plate with an angular lateral notch, and the third model represents a plate with a rectilinear lateral crack, with initial notch. On used Extended Finite Element Method (X-FEM) based on the finite element platform ABAQUS CAE. Including the aim of studying the effectiveness of the extended finite element method (X-FEM) on crack propagation.

## 2. Finite element modeling

A rectangular plate containing a lateral defect of a certain shape (semicircle, lateral notch, or crack) is studied. The size of the defect varied by changing the characteristic dimension of it. It is the radius for the semicircle type defect, it is the opening angle (the depth of the notch is considered constant) in the case of a notch and for the crack, it is its length. The dimensions of the plate considered are thickness  $e=2.5$  mm, width  $W=50$  mm and a length  $L=100$  mm. The applied load and the boundary conditions are represented in Fig. 1. The applied load  $F$  is constant traction

Table 1 Material properties of femur THR

Part of Model	Elastic Modulus (Gpa)	Poisson's Ratio
Cancellous bone	0.4	0.3
Cortical bone	$E_x, E_y=7.0, E_z=11.5$ $G_{xy}=2.6, G_{yz}, G_{zx}=3.5$	$\nu_{xy}, \nu_{zy}, \nu_{zx}=0.4$

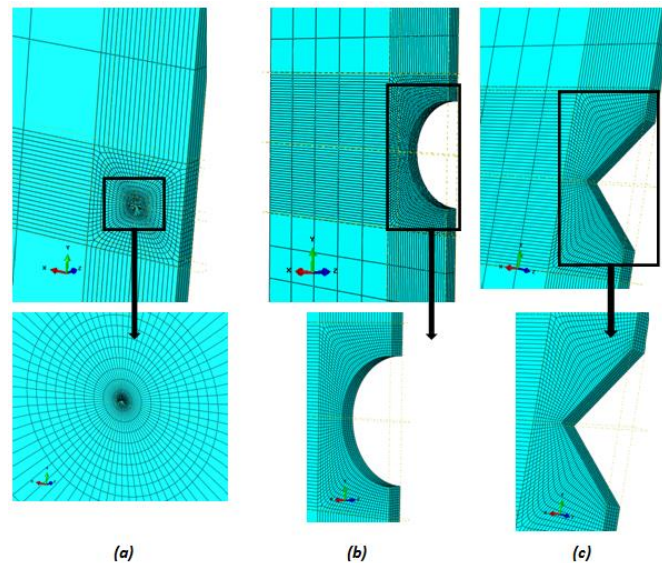


Fig. 2 Finite element meshes of the topographic model

uniformly distributed on the higher part of the plate and in the direction of the length. The value of the applied load corresponds to  $F=120$  N.

### 2.1 Material model

The plate used in this study is made of 2024T3 aluminum, a material frequently used in aeronautical structures. We considered that the behavior is elastic. Yoon *et al.* (2008). The mechanical characteristics of the model are shown in Table 1.

### 2.2 Mesh

Abaqus software has a powerful automatic mesh, which can analyze and generate the most suitable mesh. For the behavior studied, we used hexahedral elements, type C3D8 conforming to the defined parametric surfaces (Fig. 2). The mesh of the plate for various types of defects is represented in Fig. 2. It is carried out using rectangular elements with eight nodes. With regard to the semicircular defect, notch, and crack, a coarse discretization is carried out in the far zone of the defect, on the other hand, a refinement of the mesh is essential near the defect, which will make it possible to obtain a good convergence and a better accuracy of results. The mesh is made using the tools developed from the Abaqus software, and the geometry and mesh data are automatically transferred to the analysis module by the software.

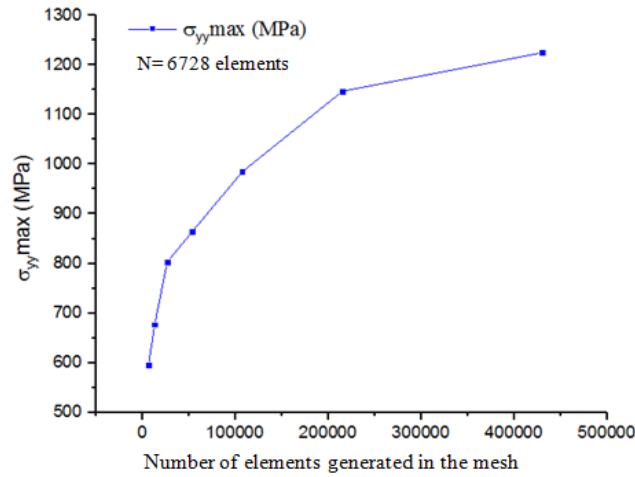


Fig. 3 Comparison between the values of the opening stress  $\sigma_{yy}$  at the bottom of the notch according to the number of elements generated for the mesh

### 2.3 Effect of the size of the element used (convergence test)

The other study of the mesh is in relation to the sizes of the elements used to generate the mesh. The realization is carried out in three dimensions with linear hexahedral elements with eight nodes. We represent in Fig. 3, the opening constraint  $\sigma_{yy}$  at the bottom of the notch for different numbers of generated elements  $N$ ,  $2N$ ,  $4N$ ,  $8N$ ,  $16N$ ,  $32N$ , and  $128N$  with  $N=6728$  elements (Fig. 3).

One note in Fig. 3, is the importance of the refinement of the mesh on the quality of the numerical results obtained. The refinement of the mesh and the increase in the elements generated in the numerical simulation converge towards the stability of the results of computation.

### 2.4 The extended finite element method (X-FEM)

The extended finite element method (X-FEM) has emerged as a powerful numerical procedure for the analysis of fracture problems. It has been widely recognized that the method facilitates the modeling of fracture growth under the assumptions of linear elastic fracture mechanics (LEFM). The fracture was modeled with the X-FEM method, which is based on the criteria of the maximum principal stress to determine the location of the initiation of the crack. This criterion is represented as follows

$$f = \begin{cases} \langle \sigma_{max} \rangle \\ \sigma_{max}^0 \end{cases} \quad (1)$$

Here  $\sigma_{max}^0$  represents the maximum authorized principal stress. The symbol  $\langle \rangle$  represents Macaulay's support with the usual interpretation

$$\langle \sigma_{max} \rangle = 0 \text{ if } \langle \sigma_{max} \rangle = \sigma_{max} \quad (2)$$

Compression stress does not initiate damage.

When  $f \geq 0$  the initiation criterion is satisfied. (Mischinski *et al.* 2013).

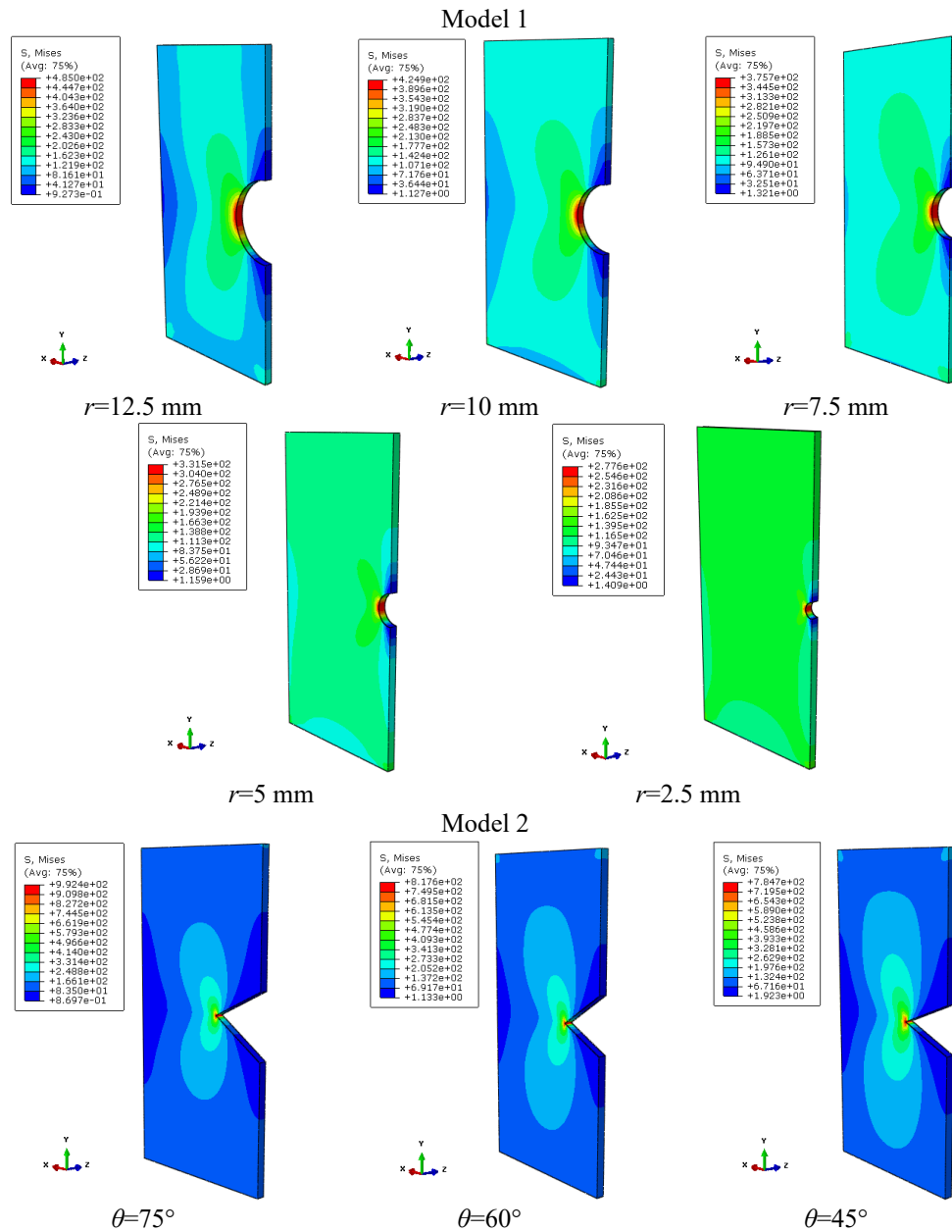


Fig. 4 Von Mises stresses distribution for different models: Model 1/semicircle with different radii; Model 2/notch with different opening angles; Model 3/crack with different lengths

### 3. Results and discussions

#### 3.1 Evolution of stresses for the different cases studied

Fig. 4 represents the Von-set stress field as a function of the radius in the case of the semi-

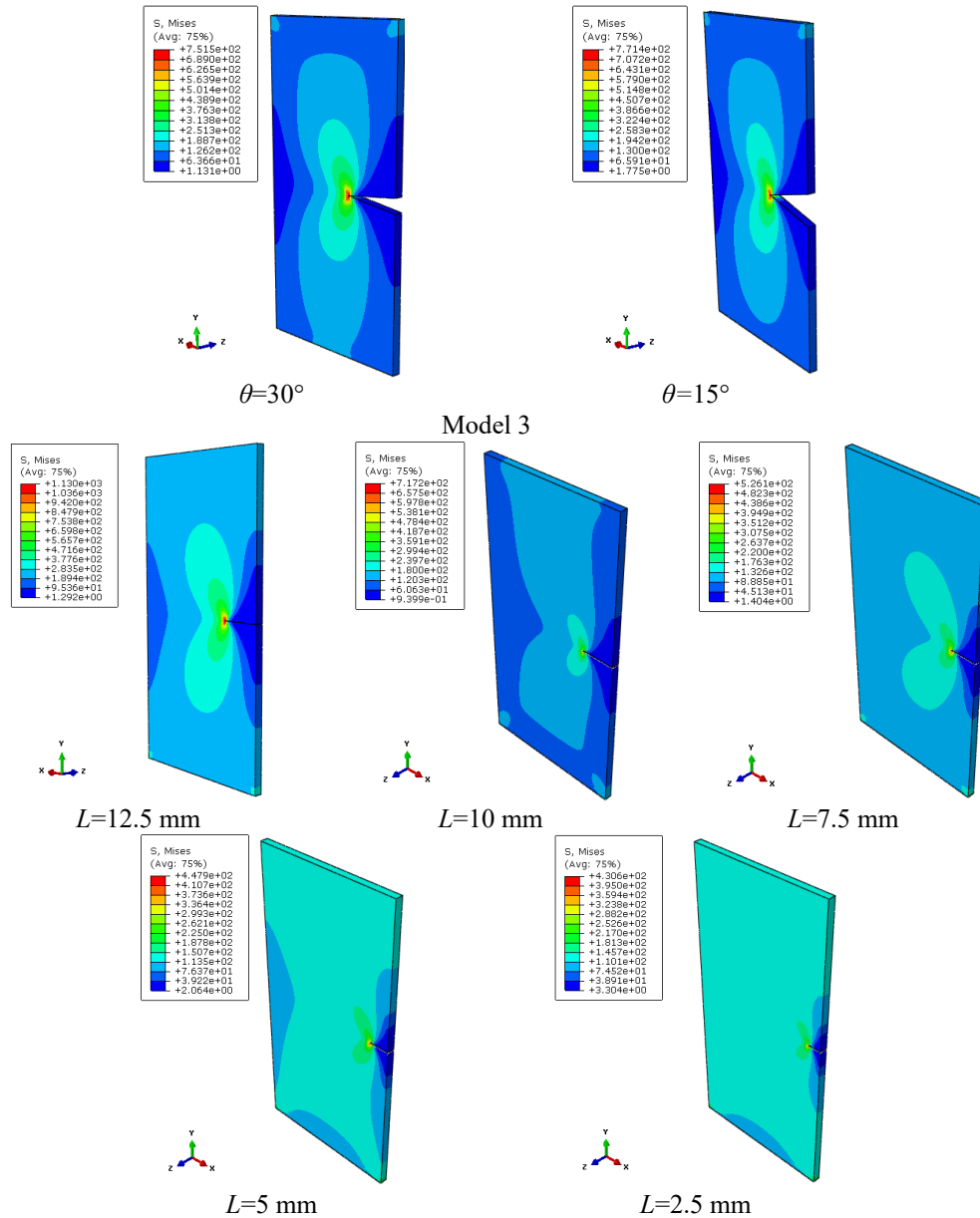


Fig. 4 Continued

circular defect (model 1), as a function of the opening angle in the case of the notch (model 2), and according to the length of the defect in the case of the crack (model 3).

Fig. 4 represents the Von-set stress field as a function of the radius in the case of the semi-circular defect (model 1), as a function of the opening angle in the case of the notch (model 2), and according to the length of the defect in the case of the crack (model 3). Fig. 4 shows the distribution of the equivalent stress of Von Mises on the surface of the plate for the various models. In the first model, we note that the stresses are concentrated at the level of the defect, this

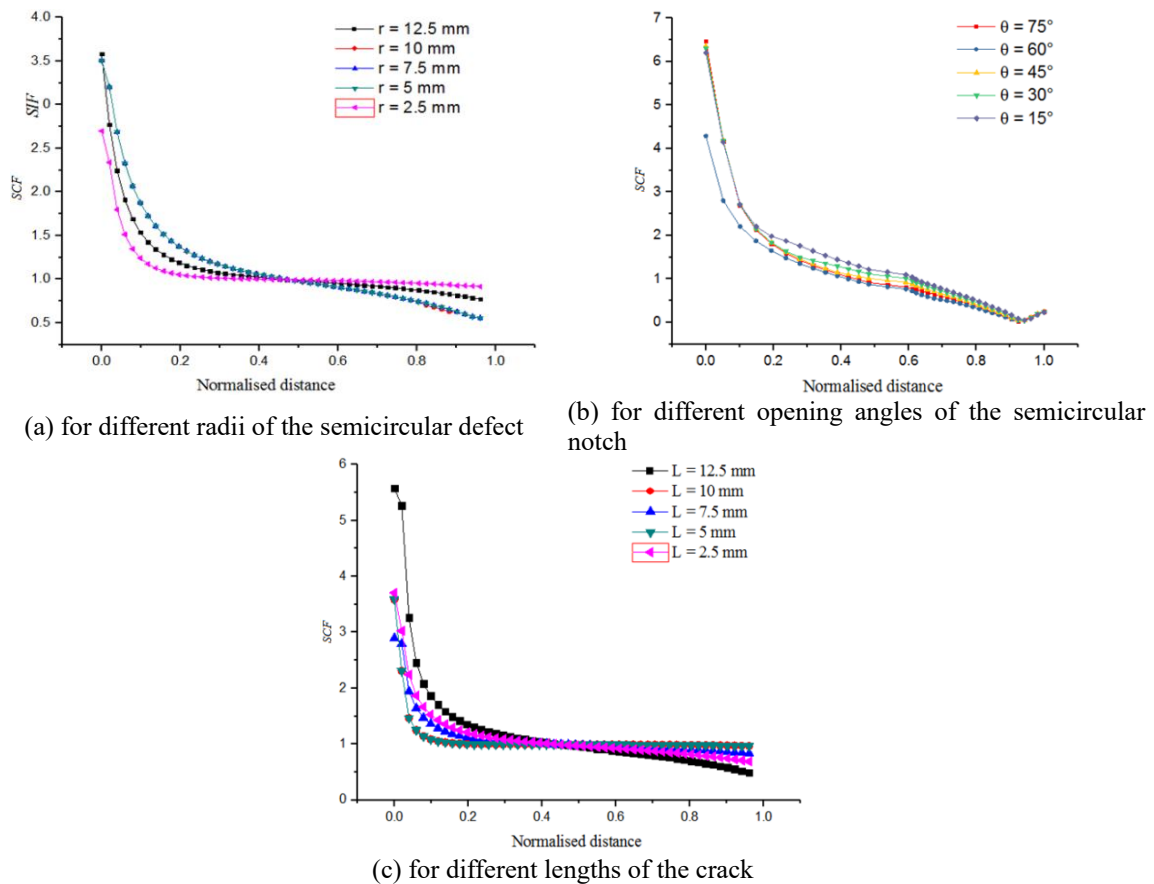


Fig. 5 Variation of the stress concentration factor  $K_t$  as function of the normalized distance

concentration decreases as one moves away from it. The stress concentration increases with the increase in the radius of the semicircle and the length of the crack. The highest stresses are located mainly near the fault. The values of the stresses are very high of the order of 485 MPa in the case radius 12.5 mm and the stresses decrease until 277 MPa with a radius 2.5 mm. In the second case of the notch (model 2) we have shown the distribution of the stresses which vary with the opening angle, it should be noted that for small opening angles, the notch tends towards a real crack (closed notch) and according to Griffith's theory, the cracks generate significant stress concentrations in the vicinity of the point. One notes that the stresses are stable and vary between 784 MPa and 751 MPa in 45-degree cases, and 15 degrees in succession. In the last model, the stresses transferred in all the regions of the plate near the defect in the form of a crack. The latter gives higher constraints than the other two models. One note is that the most intense tensile stresses are localized at the point of the crack and decrease as one moves away from this one.

### 3.2 Effect of the type of notch on the stress concentration factor $K_t$

Fig. 5 show the variation of the stress concentration factor as a function of the standard distance for the different types of fault. In the first case for a lateral semi-circular defect.

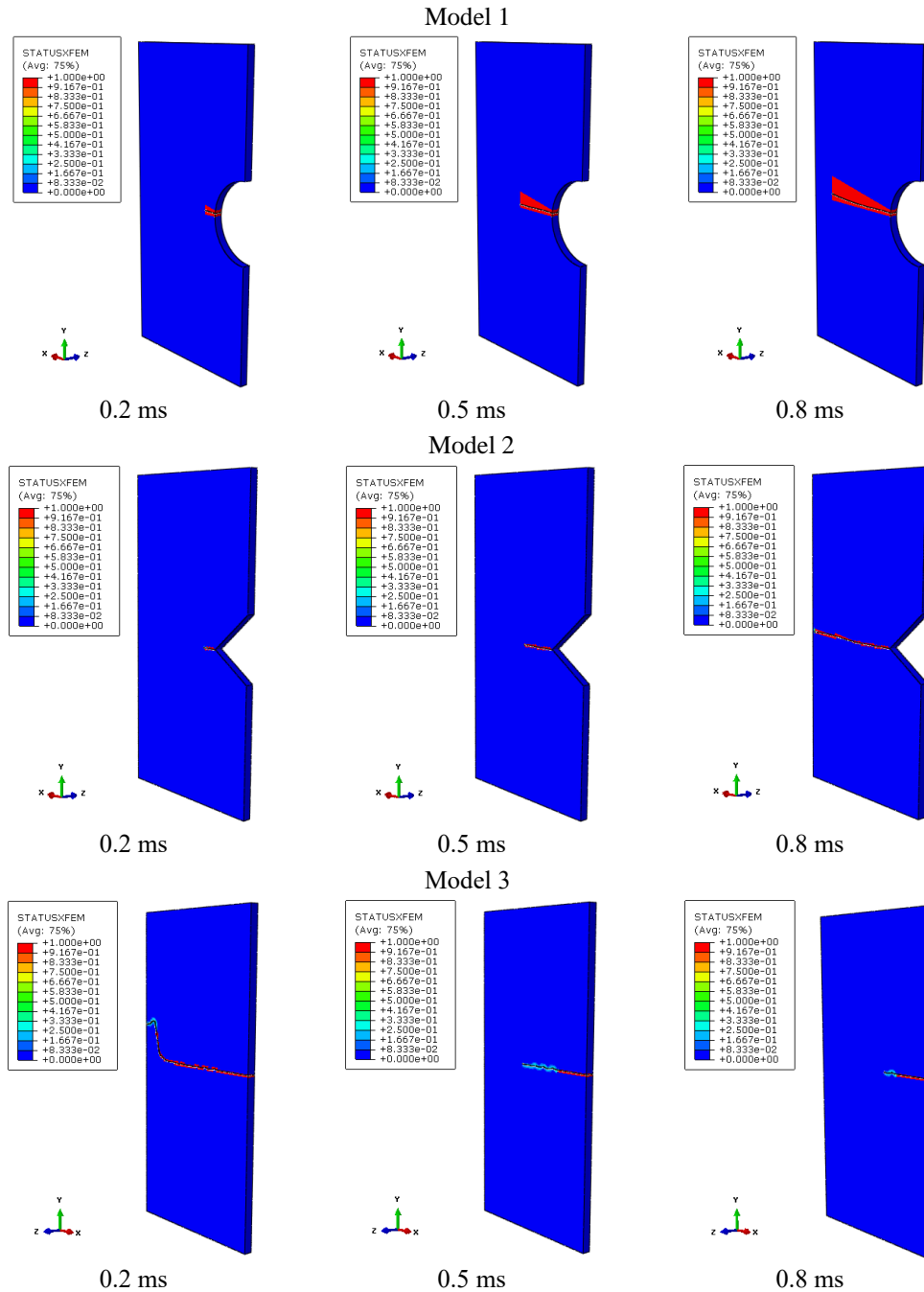


Fig. 6 Type of fracture predicted from different times for the three cases studied.

Fig. 5 represents the values of the SCF as a function of the normalized distance. The important values are in the direct vicinity of the fault, they decrease as one moves away from the latter. It noted that the larger the radius, the more the SCF values increase. For all the values of the radius,

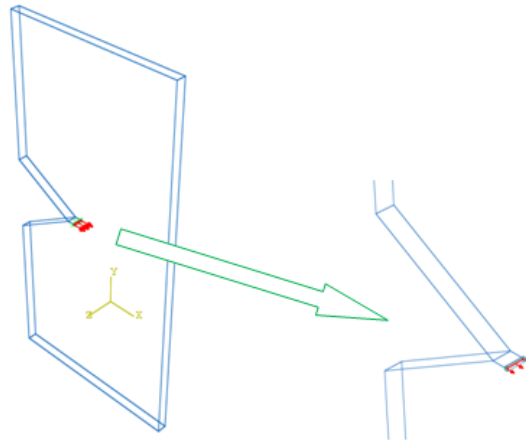
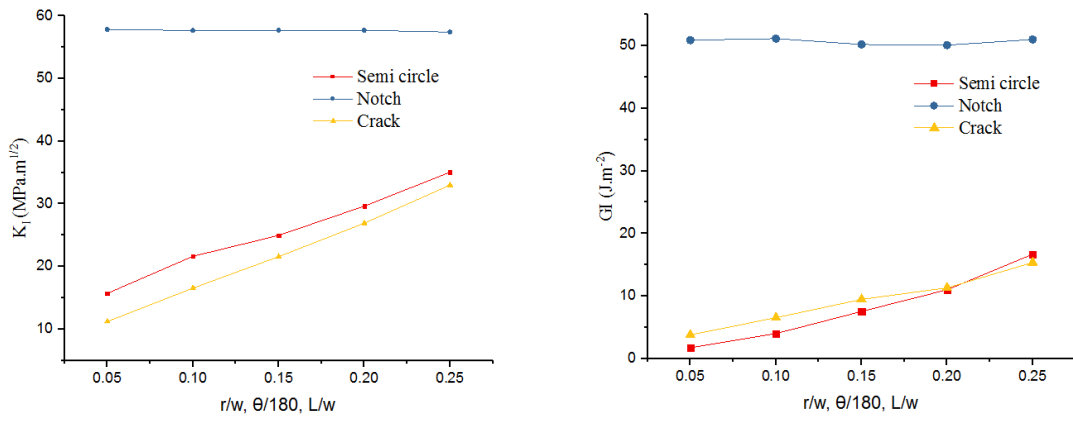


Fig. 7 The creation of a pre-crack of 2 mm: the case of the notch

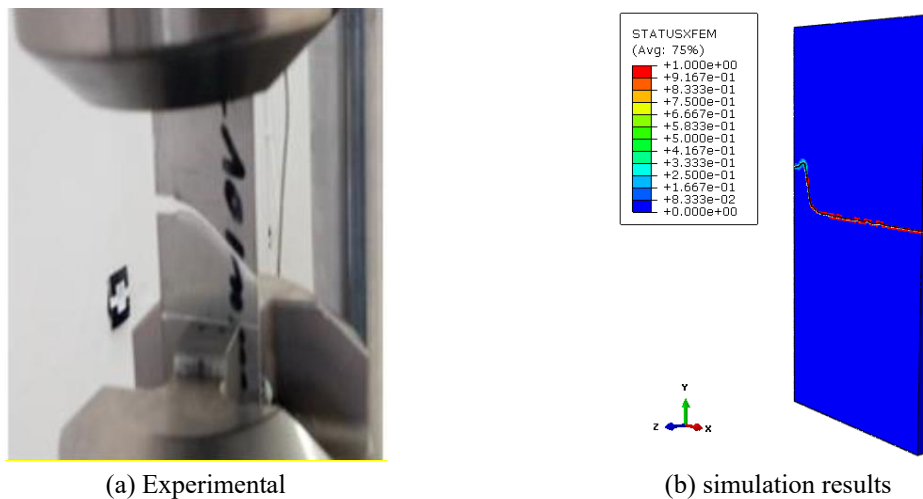
the graphs coincide in the middle of the ligament ( $r/W=0.4$ ) and tend towards close values. On the right side of the ligament the opposite is observed and the values of the calculated stresses are lower for large radii of the defect, this and due to the deformation of the plate containing a defect of the lateral semicircular type. In the second case for the notch type fault, shows the values of the component of the SCF ratio. We illustrated that the largest values are located in the vicinity of the point and are those which correspond to the notch with the smallest opening angle (in accordance with the results obtained for a crack which is considered as a closed defect), then they decrease slightly with increasing the opening angle. Note that the SCF values are very close along the ligament away from the defect. For the last case of the crack type defect, we have shown that the values of the SCF for different lengths of the crack are represented in Fig. 5. As noticed previously, in the vicinity of the point, the calculated values of SCF are weak for small lengths of the crack, the stresses then increase with the increase in the size of the crack. Far from the tip (moving away from the tip towards the right part of the ligament), the SCF values tend to approach. We can say that for a crack type defect, the stresses in the vicinity of the tip are more sensitive to the size of the defect, this sensitivity decreases while moving away from the tip.

### 3.3 Result of the X-FEM fracture

The simulation results show that the initiation and the propagation of the crack are detected by the crack X-FEM and follow its propagation in the different studied cases are represented in Fig. 6. The results of the simulation, show that with the X-FEM, on detected the initiation of crack and follow its propagation in the three deferent directions of loading (semicircle, opening angle, length of crack) the rupture is between 0.2 and 0.8 ms. On compare in a first the answers provided by a Modeling of the behaviour of the material as being elastic. As we can see in Fig. 6, the answers are almost the same; this leads to the conclusion that the confined plasticity hypothesis is particularly well suited to this type of configuration. Fig. 6 shows the damaged area in the plate near the fault for the three models, we can notice that the precedence of the damaged area (in red). On the tip of this zone, one can note a concentration of stresses. At the end of this area indicates a stress concentration. To carry out numerical calculations taking into account the process of damage to the material structure of the components of the model as well as their connections, it is necessary to



(a) Variation of the stress intensity factor KI (b) Variation in the rate of energy return GI  
 Fig. 8 the different radii and angles of the opening envisaged for the defects



(a) Experimental (b) simulation results  
 Fig. 9 Comparison between the location of the fracture

apply an appropriate numerical procedure containing parameters describing the mechanism of formation and propagation of l ‘damage. X-FEM is a method of modeling damage processes. In both cases, the elastic material with the parameters characterizing the damage to the material was defined as follows: Young’s modulus  $E=69000$  MPa, Poisson’s ratio  $\nu=0.3$ , value of the damage causing a stress in the fiber of the material  $\sigma_{max}=380$  MPa.

### 3.4 Influence of the form of the defect on the values of KI and GI

Fig. 7 shows the creation of the 2 mm long crack located at the bottom of a semicircular lateral defect and at the bottom of another notch-shaped.

Fig. 8 represents the different radii and angles of the opening envisaged for the defects of semicircular shapes and notch, respectively. The values of the stress intensity factor KI and the rate of restitution of elastic energy GI, for the two cases and the case of a lateral crack.

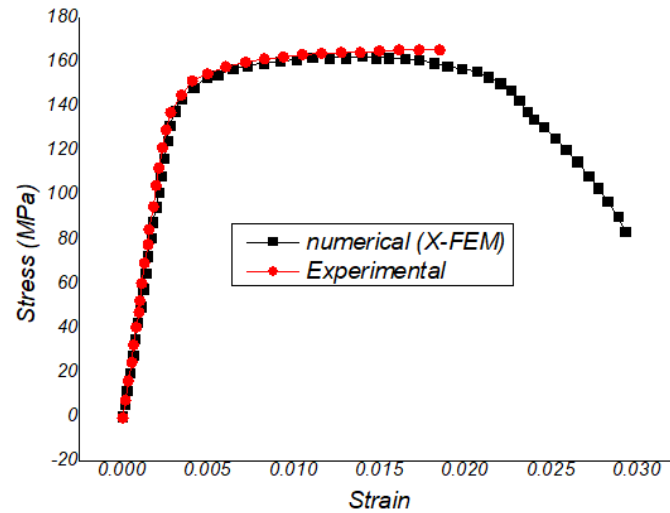


Fig. 10 Comparison between experimental and simulated results

According to Fig. 8, the stress intensity factor KI and the energy release rate GI are very sensitive to the radius of the semicircular defect and increase considerably with the latter. On the other hand, for the notch type defect, the factors KI and GI vary very little with the opening angle and they are almost constant. For the case of a lateral crack, the values of the factors KI and GI vary with the size of the crack and can reach high values compared to the other types of defects.

On comparing our numerical results (Fig. 9(b)) to experimental tests (Fig. 9(a)) directed by (Taghezout *et al.* 2020). Our numerical model presents a similarity to his experimental result. Previous results have been compared with real measurements in some cases, such as a model of a plate with an angular lateral notch or a plate with a rectilinear lateral crack. This is what justifies that X-FEM provides accurate results of plaque fracture.

In this study, a comparison graph between the experimental tensile results directed by (Taghezout *et al.* 2020) and our simulation using the extended finite element technique (X-FEM) with the ABAQUS calculation code can provide a valuable evaluation of the accuracy of the simulation method.

Fig. 10 illustrates the stress-strain curve for the experimental results performed by Taghezout *et al.* (2020), and those obtained by numerical simulation using the Abaqus 6.17 calculation software, indicating good agreement between the two curves.

#### 4. Conclusions

The present parametric study made it possible to draw conclusions on the influence of the type and size of a defect on the mechanical behavior of a thin plate subjected to a tensile force. The results obtained allowed us to conclude the following: It turns out that defects of the lateral semicircular type are defects that cause the least stress compared to the other types of defects, namely notches and cracks.

The notches are characterized by the opening angle; the stress field is more sensitive to the small opening notches in accordance with the analytical results obtained for a crack (closed notch).

The stress intensity factor KI and the energy release rate GI are very sensitive to the radius of the semi-circular defect and increase considerably with the latter.

On the other hand, for the notch-type defect, the factors KI and GI vary very little with the opening angle and we can say that they are almost constant.

For the case of a lateral crack, the values of the KI and GI factors vary with the size of the crack and can reach high values compared to other types of defects.

Lateral semicircular type defects are defects, which generate the lowest stresses compared to other types of defects.

Cracks are the defects, which have the most influence on the stress field that is very sensitive to the size of the crack.

The numerical model shows a good prediction of the shape and propagation of the crack in agreement with the X-FEM and published experimental work.

## References

- Benzaama, A., Mokhtari, M., Benzaama, H., Gouasmi, S. and Tamine, T. (2018), "Using XFEM technique to predict the damage of unidirectional CFRP composite notched under tensile load", *Adv. Aircraft Spacecraft Sci.*, **5**(1), 129. <https://doi.org/10.12989/aas.2018.5.1.129>.
- Campilho, R. and Moreira, F. (2019), "Use of the XFEM for the design of adhesively-bonded Tjoints", *Frattura ed Integrità Strutturale*, **13**(49), 435-449. <https://doi.org/10.3221/IGF-ESIS.49.40>.
- D'Angela, D. and Ercolino, M. (2021), "Fatigue crack growth in metallic components: Numerical modelling and analytical solution", *Struct. Eng. Mech.*, **79**(5), 541-556. <https://doi.org/10.12989/sem.2021.79.5.541>.
- Dorđević, B., Sedmak, S., Tanasković, D., Gajin, M. and Vučetić, F. (2021), "Failure analysis and numerical simulation of slab carrying clamps", *Frattura ed Integrità Strutturale*, **15**(55), 336-344. <https://doi.org/10.3221/IGF-ESIS.55.26>.
- Gasmi, B., Abderrahmene, S., Smail, B. and Benaoumeur, A. (2019), "Initiation and propagation of a crack in the orthopedic cement of a THR using XFEM", *Adv. Comput. Des.*, **4**(3), 295-305. <https://doi.org/10.12989/acd.2019.4.3.295>.
- Huang, X., Liu, Y., Huang, X. and Dai, Y. (2017), "Crack arrest behavior of central-cracked stiffened plates under uniform tensions", *Int. J. Mech. Sci.*, **133**, 704-719. <https://doi.org/10.1016/j.ijmecsci.2017.09.040>.
- Huang, Z., Deng, S., Li, H. and Zuo, H. (2019), "Edge crack growth of mortar plate specimens under uniaxial loading tests", *J. Rock Mech. Geotech. Eng.*, **11**(2), 300-313. <https://doi.org/10.1016/j.jrmge.2018.12.005>.
- Karamloo, M., Mazloom, M. and Ghasemi, A. (2019), "An overview of different retrofitting methods for arresting cracks in steel structures", *Struct. Monit. Mainten.*, **6**(4), 291-315. <https://doi.org/10.12989/smm.2019.6.4.291>.
- Khatri, K. and Lal, A. (2018), "Stochastic XFEM based fracture behavior and crack growth analysis of a plate with a hole emanating cracks under biaxial loading", *Theor. Appl. Fract. Mech.*, **96**, 1-22. <https://doi.org/10.1016/j.tafmec.2018.03.009>.
- Kozłowski, M., Kadela, M. and Gwozdź-Lason, M. (2016), "Numerical fracture analysis of foamed concrete beam using XFEM method", *Appl. Mech. Mater.*, **837**, 183-186. <https://doi.org/10.4028/www.scientific.net/AMM.837.183>.
- Mischinski, S. and Ural, A. (2013), "Interaction of microstructure and microcrack growth in cortical bone: a finite element study", *Comput. Meth. Biomech. Biomed. Eng.*, **16**, 81-94. <https://doi.org/10.1016/10.1080/10255842.2011.607444>.
- Nassiraei, H. and Rezaeidoost, P. (2020), "Stress concentration factors in tubular T/Y-joints strengthened with FRP subjected to compressive load in offshore structures", *Int. J. Fatig.*, **140**, 105719. <https://doi.org/10.1016/j.ijfatigue.2020.105719>.

- Nassiraei, H. and Rezadoost, P. (2021), "Parametric study and formula for SCFs of FRP-strengthened CHS T/Y-joints under out-of-plane bending load", *Ocean Eng.*, **221**, 108313. <https://doi.org/10.1016/j.oceaneng.108313>.
- Nassiraei, H. and Rezadoost, P. (2021), "SCFs in tubular X-connections retrofitted with FRP under in-plane bending load", *Compos. Struct.*, **274**, 114314. <https://doi.org/10.1016/j.compstruct.2021.114314>.
- Nassiraei, H. and Rezadoost, P. (2021), "SCFs in tubular X-joints retrofitted with FRP under out-of-plane bending moment", *Marine Struct.*, **79**, 103010. <https://doi.org/10.1016/j.marstruc.2021.103010>.
- Nassiraei, H. and Rezadoost, P. (2021), "Stress concentration factors in tubular X-connections retrofitted with FRP under compressive load", *Ocean Eng.*, **229**, 108562. <https://doi.org/10.1016/j.oceaneng.2020.108562>.
- Nassiraei, H. and Rezadoost, P. (2022), "Stress concentration factors in tubular T-joints reinforced with external ring under in-plane bending moment", *Ocean Eng.*, **266**, 112551. <https://doi.org/10.1016/j.oceaneng.2022.112551>.
- Nguyen, T.K., Phan, D.H., Phan, T.T. and Phan, A.V. (2018), "Symmetric Galerkin boundary element analysis of the interaction between multiple growing cracks in infinite domains", *Arch. Appl. Mech.*, **88**, 2003-2016. <https://doi.org/10.1007/s00419-018-1430-6>.
- Pathak, H., Singh, A., Singh, I.V. and Yadav, S.K. (2013), "A simple and efficient XFEM approach for 3-D cracks simulations", *Int. J. Fract.*, **181**, 189-208. <https://doi.org/10.1007/s10704-013-9835-2>.
- Pereira, S.A.G., Tavares, S.M. and de Castro, P.M. (2019), "Mixed mode fracture: Numerical evaluation and experimental validation using PMMA specimens", *Frattura ed Integrità Strutturale*, **13**(49), 412-428. <https://doi.org/10.3221/IGF-ESIS.49.40>.
- Sedmak, A. (2016), "Fatigue life prediction of casing welded pipes by using the extended finite element method", *Frattura ed Integrità Strutturale*, **10**(36), 46-54. <https://doi.org/10.3221/IGF-ESIS.36.05>.
- Srivastava, A.K., Arora, P.K. and Kumar, H. (2016), "Numerical and experiment fracture modeling for multiple cracks of a finite aluminum plate", *Int. J. Mech. Sci.*, **110**, 1-13. <https://doi.org/10.1016/j.ijmecsci.2016.02.010>.
- Taghezout, A., Mostefa, B., Djebli, A., Abdelkarim, A. and Khellafi, H. (2020), "Experimental and numerical fracture modeling using XFEM of aluminum plates", *Int. J. Eng. Res. Africa*, **46**, 45-52. <https://doi.org/10.4028/www.scientific.net/JERA.46.45>.
- Yoon, Y.J. and Cowin, S.C. (2008), "An estimate of anisotropic poroelastic constants of an osteon", *Biomech. Model. Mechanobiol.*, **7**(1), 13-26. <https://doi.org/10.1016/10.1007/s10237-006-0071-9>.

CC

## Nomenclature

$E$	: Young Modulus
$\theta$	: notch angle
$r$	: notch radius of semicircular notch
$KI$	: Stress intensity factors
$\sigma_{\max}$	: The maximum authorized principal stress
GI	: The rate of restitution of elastic energy
SCF	: Stress concentration factor
X-FEM	: Extended finite element method